Using Spiral Intensity Profile to Quantify Head and Neck Cancer

Koon Y. Kong, Yachna Sharma, S. Hussain Raza, Zhuo (Georgia) Chen,
Susan Muller and May D. Wang

***Abstract*—During the analysis of microscopy images, researchers locate regions of interest (ROI) and extract relevant information within it. Identifying the ROI is mostly done manually and subjectively by pathologists. Computer algorithms could help in reducing their workload and improve reproducibility. In particular, we want to assess the validity of the folic acid receptor as a biomarker for head and neck cancer. We are only interested in folic acid receptors appearing in *cancerous tissue*. Therefore, the first step is to segment images into cancerous and noncancerous regions. We propose to use a spiral intensity profile for segmentation of light microscopy images.**

Many algorithms identify objects in an image by considering pixel intensity and spatial information separately. Our algorithm integrates intensity and spatial information by considering the change, or profile, of pixel intensity in a spiral fashion. Using a spiral intensity profile can also perform segmentation at different scales from cancer regions to nuclei cluster to individual nuclei. We compared our algorithm with manually segmented image and obtained a specificity of 83.7% and sensitivity of 61.1%. Spiral intensity profiles can be used as a feature to improve other segmentation algorithms. Segmentation of cancerous images at different scales allows effective quantification of folic acid receptor inside cancerous regions, nuclei clusters, or individual cells.

I. Introduction

Cancer has become the top killer for Americans under the age 85, surpassing heart disease. Although some risk factors, or biomarkers, have been identified, a large number remain unknown. Additional biomarkers could help physicians provide a more accurate cancer prognosis. We are interested in investigating whether folic acid receptors can be used as a potential biomarker for head and neck cancer.

Pathologists grade patient tissue slides under conventional light microscope after staining with appropriate chemical dyes or immunohistochemistry. Analyses of these tissue slides include cancer classification, identification of cancer clusters, and assessment of folic acid receptor expression intensity. Traditionally, these tasks are performed subjectively by trained pathologists. Typical protocols require pathologists to look at each slide and record receptor expression by assigning a grade. The task is time-consuming and tedious. With the aid of high resolution digital photography, tissue slides can be stored digitally. Robust image analysis algorithms are highly desirable to manage this information and reduce the amount of labor along with increased reproducibility.

To analyze the folic acid receptor expression from a head and neck cancer tissue sample, regions of cancerous cell are first identified and segmented. These regions of interests (ROIs) are what pathologists consider during the grading process. The amount of expression is obtained by judging the intensity of the stain within these ROIs. Usually, grading of zero to three is assigned based on the total intensity of stain expressed within the identified cancer regions. The first step for an automated computer algorithm is to segment the ROIs from tissue slide images. In this paper, we propose the use of a spiral intensity profile to achieve segmentation of ROIs. It provides a single feature that integrates spatial and intensity information. Our approach allows fully automatic hierarchical segmentation at different levels (*i.e.,* cancerous region marking, segmentation of cell/nuclei aggregates, and individual cell/nuclei segmentation).

II. Background

For automatic quantification of folic acid receptor expression, we need to distinguish normal regions from cancerous regions. Several research endeavors pertaining to segmentation rely on blob detection and sub-image segmentation. Hinz [1] assumes each blob is a rectangular step function and detects the center of each blob by locating the maximum curvature along the width and length direction of the rectangle. The Hessian matrix defines the orientation of rectangles. Jiang et al. [2] extracts cytoplasm and nuclei of white blood cells using two different methods: scale space filtering to segment the nuclei and watershed clustering to segment the cytoplasm. Morphological anisotropic diffusion, and moving interface models segment leukocytes in [3] and [4], respectively. Lamberti and Montrucchio [5] use multistage segmentation technique for classification of blood vessels. It identifies the most probable cell locations using cell brightness and morphology segments Hematopoietic

Manuscript received June 15, 2008. This work was supported in part by grants from National Institutes of Health (Bioengineering Research Partnership R01CA108468, P20GM072069, Center for Cancer Nanotechnology Excellence U54CA119338), Georgia Cancer Coalition (Distinguished Cancer Scholar Award to Professor Wang), Hewlett Packard, and Microsoft Research.

Koon Yin Kong is with the Georgia Institute of Technology, Atlanta, GA 30332 USA (e-mail: kykong@gatech.edu).

Yachna Sharma is with the Georgia Institute of Technology, Atlanta, GA 30332 USA (e-mail: ysharma3@gatech.edu).

Syed Hussain Raza is with the Georgia Institute of Technology, Atlanta, GA 30332 USA (e-mail: hussain.raza@gatech.edu).

Zhuo (Georgia) Chen is with the Emory University, Atlanta, GA 30332 USA (e-mail: gzchen@emory.edu).

Susan Muller is with the Emory University (e-mail: susan.muller@emoryhealthcare.org)

May Wang is with Georgia Tech and Emory University, Atlanta, GA 30332 USA (e-mail: maywang@bme.gatech.edu).

Stem Cells (HSCs) [6]. Ben Sheh [7] uses geodesic reconstruction to segment drusen in eye fundus images and also proposes direct classifications of cancer cells. DBSCAN (density-based algorithm for discovering clusters in large spatial databases with noise) and a support vector machine (SVM) segments head and neck cancer cells in [8].

Most of the blob detection and other segmentation approaches described above assume small intensity variation within each blob or region. This is not necessarily the case for our data set because the image is acquired from a microscope with different illumination and staining within each slide. Heterogeneity of cancer cells also makes that assumption less likely to be true. Furthermore, most algorithms consider pixel intensity and spatial information separately. We propose to look at intensity variations in a spiral fashion to integrate both intensity and spatial information. Our algorithm is designed to perform ROI segmentation at different scales and is capable of handling the intensity variations and tissue heterogeneity.

III. METHODOLOGY

A block diagram of the overall methodology is shown in Figure 1. A spiral intensity profile is constructed for each pixel in the down-sampled image. Those profiles are smoothed and k-mean clustering algorithm is used to classify into different clusters. Individual cluster represents segmented cancer region.

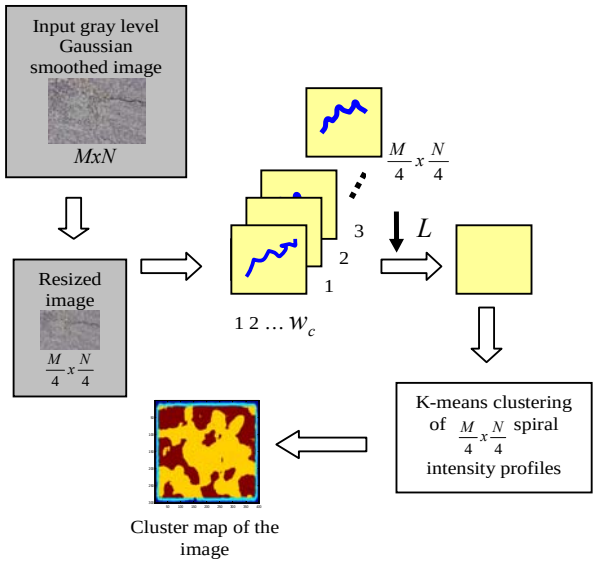

Fig 1. Overall methodology.

A. Image Enhancement

Since the biopsy tissue image is captured with lighting provided through back projection, most pixels have high intensity values. First, we convert the RGB images to gray scale images. Histogram equalization is performed to utilize the full intensity range of each pixel. Low pass filtering with a Gaussian kernel of size 5x5 is used to smooth out local intensity variations. The input image is 1600x1200 in size. To reduce computation time, the image is down sampled by 4.

B. Spiral Profile

We propose to un-wrap pixels in a spiral to form the spiral intensity profile. A spiral intensity profile is constructed for each pixel in an image. This is done by reordering neighborhood pixels so that their spatial locations form a clockwise spiral originating from the central. The re-organization of a 5 x 5 neighborhood (w_c = 2) in a spiral fashion is shown in Figure 2.

$I_{(x-2,y-2)}$ **22**	$I_{(x-1,y-2)}$ **15**	$I_{(x,y-2)}$ **10**	$I_{(x+1,y-2)}$ **16**	$I_{(x+2,y-2)}$ **23**
$I_{(x-2,y-1)}$ **14**	$I_{(x-1,y-1)}$ **6**	$I_{(x,y-1)}$ **2**	$I_{(x+1,y-1)}$ **7**	$I_{(x+2,y-1)}$ **17**
$I_{(x-2,y)}$ **13**	$I_{(x-1,y)}$ **5**	$I_{(x,y)}$ **1**	$I_{(x+1,y)}$ **3**	$I_{(x+2,y)}$ **11**
$I_{(x-2,y+1)}$ **21**	$I_{(x-1,y+1)}$ **9**	$I_{(x,y+1)}$ **4**	$I_{(x+1,y+1)}$ **8**	$I_{(x+2,y+1)}$ **18**
$I_{(x-2,y+2)}$ **25**	$I_{(x-1,y+2)}$ **20**	$I_{(x,y+2)}$ **12**	$I_{(x+1,y+2)}$ **19**	$I_{(x+2,y+2)}$ **24**

Fig 2. Relationship between pixel location, $I_{(u,v)}$, and pixel order, blue/bold indexes, of a 5x5 spiral.

If, $I_{(x,y)}$ is the intensity of the central pixel in the neighborhood, then a spiral sequence is generated starting from the central pixel in a clockwise manner. For example, in Figure 2, $I_{(x,y+1)}$ indicates that the intensity of the pixel at $(x,y+1)$ occurs at the fourth position in the spiral intensity profile. Each pixel of the input image is treated as the central pixel with zero padding for pixels lying on the input image edges. For each intensity profile, we compute the distance and angle from all the pixels in a neighborhood of size w_c. The distance r is calculated for each neighboring pixel with respect the center pixel (x_c, y_c) within the neighborhood w_c.

$$r = \sqrt{\left((x_c - x)^2 + (y_c - y)^2\right)}; x, y \in w_c \qquad (1)$$

The angle θ is the angle between the central pixel and the neighboring pixels within a neighborhood of size w_c and is given by

$$\theta = \tan^{-1}\left(\frac{y - y_c}{x - x_c}\right) \qquad (2)$$

Figure 3 shows the graphical representation of the angle and distance.

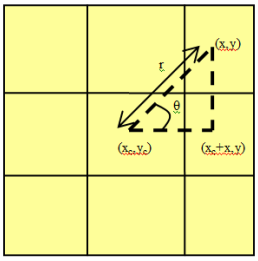

Fig 3. Distance and angle calculation for spiral profile.

We sort r in ascending order, and for terms with the same value of r, we further sort them according to the angle θ.

$$l = (r_1,\theta_1),(r_2,\theta_2),\ldots,(r_n,\theta_n) \quad \begin{cases} r_i \le r_{i+1} \\ if \quad r_i = r_{i+1} \\ then \quad \theta_i \le \theta_{i+1} \end{cases} \qquad (3)$$

The sorted sequence of intensity values in the neighborhood gives the spiral intensity profile, $S(x_c, y_c)$, for the central pixel at (x_c, y_c) within the neighborhood w_c. Figure 4 shows the

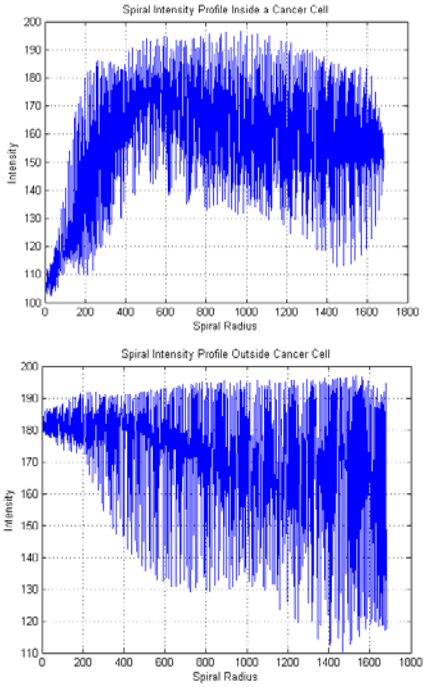

Fig 4. Top: spiral intensity profile of locations inside the cancerous region; Bottom: outside the cancerous region.

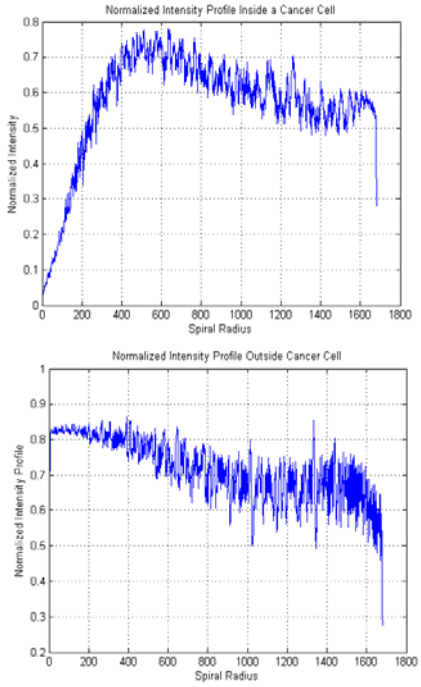

Fig 5. Top: Normalized intensity profile of locations inside the cancerous region; Bottom: outside the cancerous region.

spiral intensity profiles of two pixels inside and outside the cancerous region.

C. Cancer Cell Classification

From the two spiral intensity profiles in Figure 4, we see that the profile changes significantly for pixels inside and outside of a cancer cell. To account for the high-frequency noise introduced from pixels that are far away from the center of the spiral, an eleven-point moving average filter is applied. The intensity level is also normalized to the interval [0, 1]. Figure 5 shows the result of the smoothed and normalized spiral intensity profiles. From the two normalized intensity profiles, we see that similar regions would likely have similar spiral intensity profiles. We exploit this characteristic by applying a simple 4-class k-means algorithm to cluster the spiral intensity profiles into different classes. We use the result from the k-means clustering as a mask to segment out the cancerous region from background. By varying the neighborhood size w_c, we are able to apply the same algorithm for finer segmentation of cancerous regions into nuclei clusters and individual nuclei.

IV. Biopsy / Image Acquisition

The folic acid receptor (FR) expression in tissue specimens is determined using a goat anti-human FR polyclonal antibody (sc-16387, 1:100 dilution; Santa Cruz Biotechnology, Santa Cruz, CA, USA). Goat IgG at 1:100 dilutions is used as a negative control. Immunohistochemical analysis of formalin-fixed, paraffin-embedded human specimens is performed according to a modified procedure. In brief, after deparaffinization with xylene and rehydration with EtOH, endogenous peroxidase activity is blocked by incubating the slides in 3% hydrogen peroxide with methanol for 15 minutes. To retrieve the antigens, the tissue slides are heated in a microwave oven in 100M sodium citrate buffer (pH 6.0) for 10 minutes and then allowed to remain at room temperature for 20 minutes. After washing in PBS, the slides are incubated with serum blocking solution (2.5% normal horse serum, Vector Laboratories, Burlingame, CA) containing Avidin (Blocking Kit, Vector Laboratories) for 30 minutes to decrease the background signal. Next, the slides are incubated with a 1:100 dilution of anti FR primary antibody at 4˚C overnight, and washed with PBS. Then the slides are incubated with a biotinylated secondary antibody for 20 minutes at room temperature and with biotin-avidin peroxidase conjugate (ABC kit, Vector Laboratories) for 15 minutes at room temperature. The substrate is then added (0.1% 3.3'-diaminobenzidine solution, Sigma Chemical Co., St. Louis, MO, in PBS with 0.01% hydrogen peroxide) for 5 minutes. Finally, the slides are counterstained with hematoxylin for 50 seconds (Vector laboratories) and then observed by light microscopy.

All images are captured using Optronics MicroFIRE True Color Firewire Microscope Digital CCD Camera. Ten images are captured per slide at 200X magnification. Those images are color balanced automatically with vendor provided software. The camera is set to have shutter speed of 25ms and gain of 3.

V. Result

We apply the proposed algorithm to process head and neck

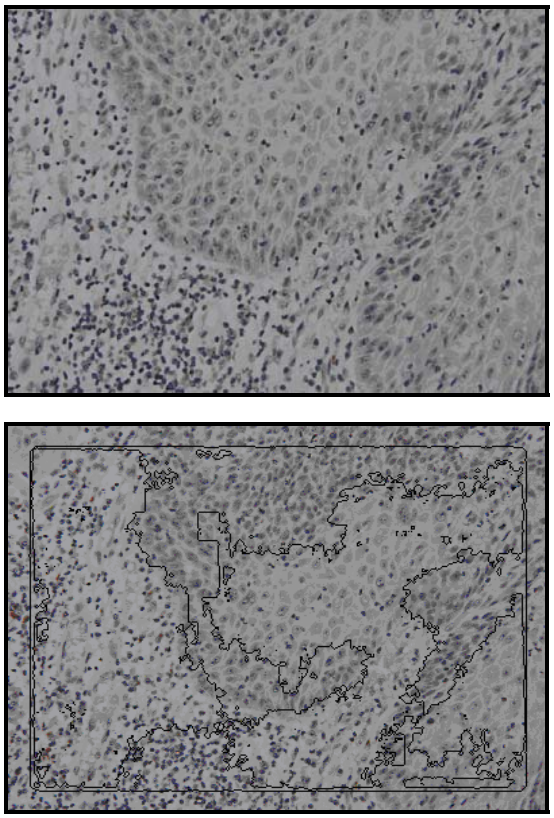

Fig 6. Top: original image; Bottom: marked image.

cancer tissue images. The size of original image is 1600x1200 pixels. Each pixel contains a 24-bit value with 8 bit corresponding to red, green and blue planes. To reduce the computation time, we down sample the image by 4, so that the image size is 400x300 pixels.

An original head and neck cancer tissue image, along with the segmented results showing the marking of cancerous regions is shown in Figure 6. The two rectangular bands along the image boundary are formed due to zero padding of the boundary pixels. The spiral intensity profile of these bands is different from the cancerous and noncancerous regions and thus appears as two separate clusters using the k-means algorithm.

The result for the center portion of the biopsy is shown in Figure 7. The edge is removed to show only relevant data. Our algorithm successfully segments cells with different shapes and sizes corresponding to both normal and cancer cells in spite of these morphological variations.

Segmented results for another image are presented in Figure 8 along with pathologist marked gold standard. We have 30 images that are manually marked. We estimate the specificity by calculating the difference in area between the gold standard and our results, assuming that the gold standard is the positive case. Overall, the algorithm achieves specificity of 83.73% and sensitivity of 61.12%. It can be seen that our results correspond well with the gold standard from the pathologist except that the partial necrotic or differential regions inside the cancerous areas are also marked by our algorithm and rectangular bands along the

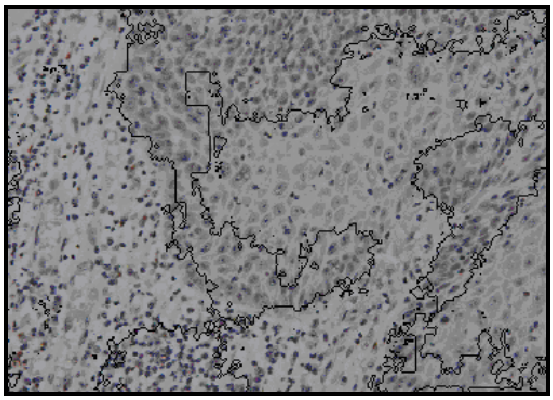

Fig 7. Result for the central portion of the image in Fig 6.

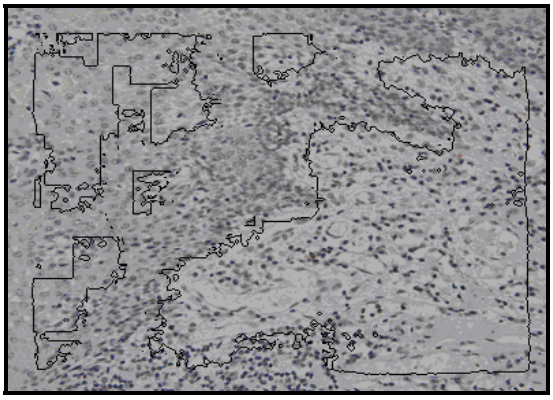

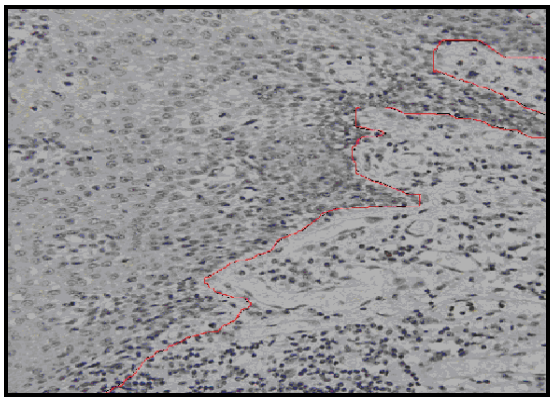

Fig 8. Top: image marked by our algorithm; Bottom: image marked by pathologist (gold standard).

image boundary occur due to zero padding as mentioned before. Marking of cancerous regions is obtained with w_c= 20 and segmentation of nuclei clusters is obtained with w_c= 10. Individual nuclei can be segmented using w_c= 5. This demonstrates that our algorithm can be effectively used for segmentation at different levels and subsequent quantification of folic acid receptor at each level of segmentation. Results at multiple level of segmentation are shown in Figure 9, 10, and 11 for different neighborhood values of w_c. With a neighborhood window size of five, we are able to segment individual nuclei, however, as the window size increases the cluster map evolves into a cancerous versus noncancerous mask.

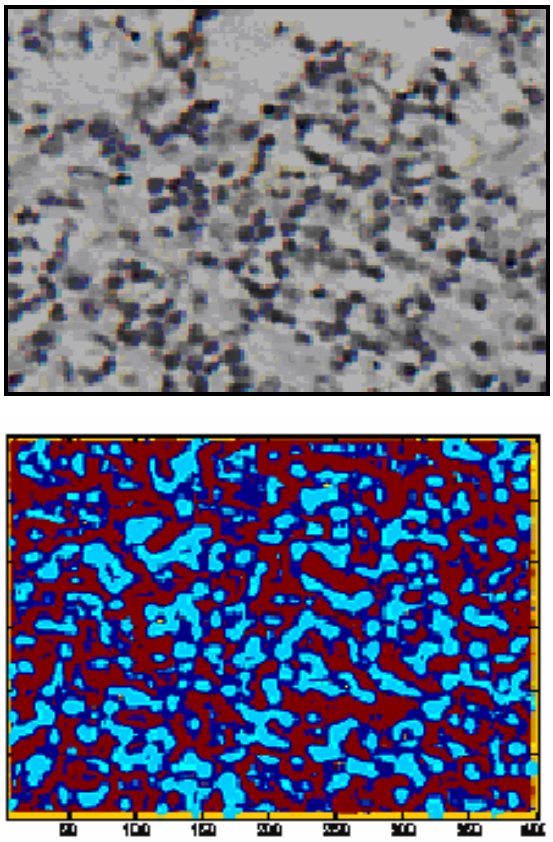

Fig 9a. Top: input image; Bottom: cluster map with w_c=5.

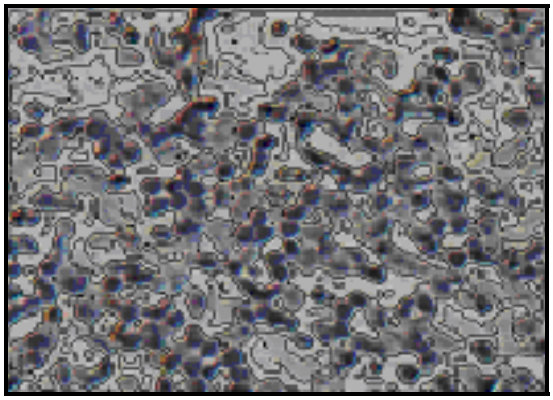

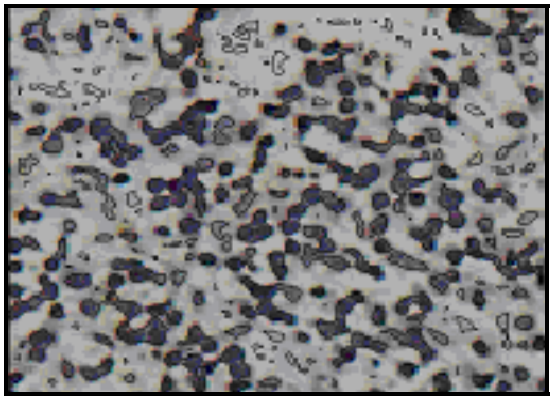

Fig 9b. Top: segmented nuclei aggregates; Bottom: individual segmented nuclei with w_c =5.

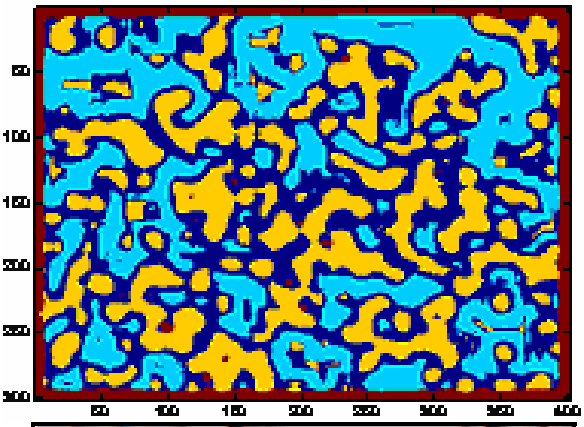

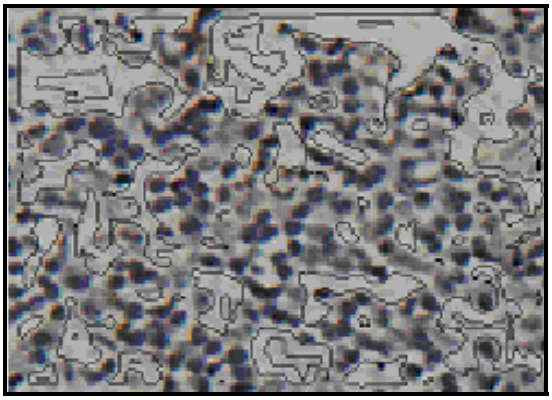

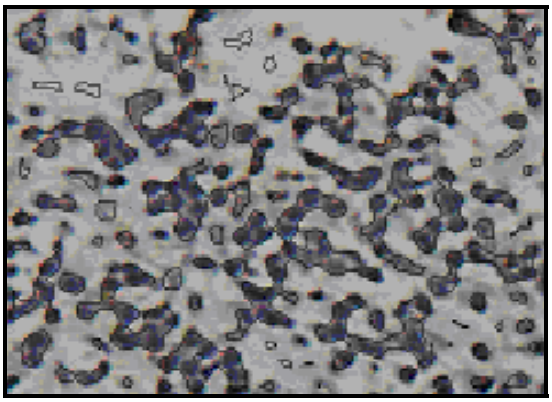

Fig 10. Top: cluster map; Middle: segmented nuclei regions; Bottom: nuclei aggregates with w_c =10.

VI. DISCUSSION AND FUTURE WORK

We show that considering the intensity pattern in a spiral fashion could help identify regions of interest in head and neck cancer tissue images. Spiral intensity profiles integrate both pixel intensity information and spatial information about its neighbors. Our algorithm works best when the cell is circular, because we use a symmetric spiral. This is mostly true when quantifying head and neck cancer tissue images. To apply our algorithm on other types of cells, the shape of the spiral can be changed. For instance, different spirals can be obtained using a rectangular neighborhood area instead of a square neighborhood. This will give the elliptical spiral which may be suitable for cell with other shaped.

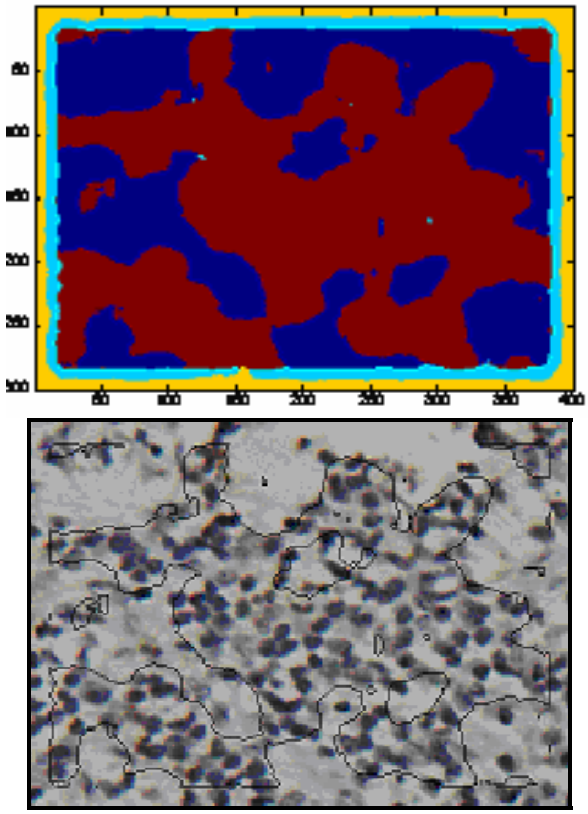

Fig 11. Top: cluster map; Bottom: segmented cancerous regions with w_c =20.

In some of the results, we see the edge effects. The edges at the boundary of cancerous and noncancerous regions appear as straight lines instead of following the region contours as shown in Figure 12. This straightening effect is more prominent with large neighborhood size w_c and can be attributed to the insufficient spatial resolution that results due to aliasing caused by down sampling the image. Aliasing can be prevented in three ways: 1) Using a higher sampling frequency; 2) Low-pass filtering the image to obtain a band limited signal; 3) Block processing the whole image to preserve spatial resolution. We could overcome this effect by block processing the image data instead of down sampling the image. The whole image (1600x1200) can be divided into sixteen blocks of size 400x300 and each block is processed individually. This would reduce the aliasing effect; however, the computation time will increase.

The classification of cancer cell regions is fully automatic, so the speed of the algorithm is less of an issue because it can be computed offline. However, the algorithm speed could be improved for real-time use by using methods like an image pyramid. Since we are able to segment the biopsy image, future work will involve folic acid receptor quantification for different segmentation levels. We would be able to provide a quantitative measure of the folic acid receptor expression for the whole cancerous region, nuclei/cell clusters and for single nuclei and cells. Also, we will test our algorithm for biopsy images of other cancer types.

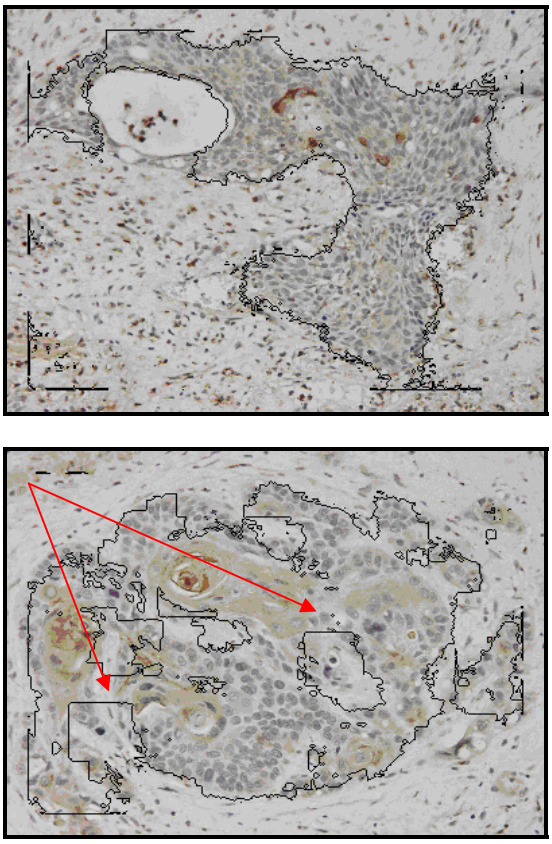

Fig 12. Edge effect located on the boundary of cancer and noncancerous regions. Arrows indicate the areas where straight edges occur in segmented regions.

REFERENCES

[1] S. Hinz, "Fast and Sub pixel Precise Blob Detection and Attribution", Processing IEEE International Conference on Image, 2005, vol. 3, pp: 457-460.

[2] K. Jiang, Q. M. Liao, S. Y. Dai, "A novel white blood cell segmentation scheme using scale-space filtering and watershed clustering", International Conference on Machine Learning and Cybernetics, 2-5 Nov. 2003, pp:2820 - 2825, Vol.5.

[3] S. T. Acton, K. Ley, "Tracking leukocytes from in vivo video microscopy using morphological anisotropic diffusion", Proceedings 2001 International Conference on Image Processing, 7-10 Oct. 2001, pp: 300-303, vol.2.

[4] B. Nilsson, A. Heyden, "Model-based segmentation of leukocytes clusters", 16th International Conference on Pattern Recognition, 2002. Proceedings, Volume 1, 11-15 Aug. 2002, pp: 727-730, vol.1.

[5] F. Lamberti, B. Montrucchio, "Segmentation of in-vitro endothelial cell networks", IEEE International Symposium on Biomedical Imaging: Macro to Nano, 2004., 15-18 April 2004, pp: 129-132, Vol. 1.

[6] N. N. Kachouie, L. J. Lee, P. Fieguth, "A Probabilistic Living Cell Segmentation Model", IEEE International Conference on Image Processing, 2005. Volume 1, 11-14 Sept. 2005, pp: 1137-1140.

[7] Z. Ben Sbeh, L. D. Cohen, G. Mimoun, G. Coscas, "A new approach of geodesic reconstruction for drusen segmentation in eye fundus images", IEEE Transactions on Medical Imaging, Volume 20, Issue 12, Dec. 2001, pp:1321-1333.

[8] M. Mete, X. Xu, C. Fan, and G. Shafirstein, “Head and Neck Cancer Detection in Histopathological Slides”, Sixth IEEE International Conference on Data Mining Workshops, Dec. 2006, pp: 223 – 230.